Force correction analysis method for derivation of multidimensional free energy landscapes from adaptively-biased replica simulations

Fabrizio Marinelli[1]* and José D. Faraldo-Gómez [1]*

[1]Theoretical Molecular Biophysics Laboratory
National Heart, Lung and Blood Institute
National Institutes of Health, Bethesda, MD 20814

*Correspondence should be addressed to:
Fabrizio Marinelli or José D. Faraldo-Gómez
E-mail: fabrizio.marinelli@nih.gov , jose.faraldo@nih.gov

May 18, 2021

Abstract

A methodology is proposed for calculating multidimensional free-energy landscapes of molecular systems, based on post-hoc analysis of multiple molecular dynamics trajectories wherein adaptive biases are used to enhance the sampling of different collective variables. In this approach, which we refer to as Force Correction Analysis Method (FCAM), total and biasing forces from all trajectories are subtracted and combined in the form of local averages, so as to obtain unbiased estimates of the mean forces across collective-variable space; multidimensional free-energy surfaces and minimum-energy pathways are then derived from integration of the mean forces through kinetic Monte Carlo simulations. Numerical tests for trajectories of butyramide generated with standard and concurrent metadynamics, biased to sample one and two dihedral angles, respectively, as well as metadynamics simulations of deca-L-alanine reversible unfolding, demonstrate the correctness of the method and show that calculated mean forces and free energies converge rapidly. Analysis of bias-exchange metadynamics simulations of dialanine, trialanine and the SH2-SH3 domain-tandem of the Abl kinase, using up to six collective-variables, further demonstrate this approach greatly facilitates calculating accurate multidimensional free-energy landscapes from different trajectories and time-dependent biases, outperforming other post-hoc unbiasing methods.

Introduction

Molecular dynamics (MD) simulations are an increasingly powerful tool to investigate complex chemical and biological mechanisms, and a means to formulate atomically detailed and physically coherent interpretations of experimental measurements[1, 2]. Too often, however, simulation studies aspire to characterize slow processes using basic algorithms, typically resulting in largely anecdotal observations and dubious mechanistic inferences[3]. Biased-sampling techniques, by contrast, can yield quantitative information even for slow processes, provided the calculations are designed thoughtfully and analyzed rigorously. This information is ideally in the form of a landscape mapping the free energy of the molecular system as a function of one or more structural descriptors of the process of interest, formulated ad-hoc, and often referred to as collective variables (CVs)[4-7]. The minima and barriers in this landscape intuitively represent the most probable states of the molecular system and the transition pathways that connect them, thus explaining the emergence of a mechanism[8-12]. Among a variety of existing biased-sampling techniques, some of the most widely used are umbrella sampling (US) [13], adaptive-biasing force (ABF) [14-16] and metadynamics[17-19]. These three methods are alike in that they influence the exploration of collective-variable space by introducing biasing forces in the calculation of atomic trajectories; however, while in US these forces depend solely on the instantaneous molecular configuration, in Metadynamics and ABF they change gradually over the course of a simulation as the target space is increasingly explored, i.e. these methods are adaptive. This adaptability is arguably advantageous, although it makes rigorous derivation of free-energies more complex, from a theoretical standpoint[16, 19]. An additional difficulty is that it is non-trivial to identify *a priori* what CVs might be the most suitable for the problem at hand; it is not uncommon for intuitive descriptors to be entirely ineffective as drivers of configurational sampling. This difficulty has led to the development of specialized techniques based on reaction coordinates optimization[20-24] or enhanced biasing protocols that allow using different possible CVs, through single [25, 26] or multiple biases[27] and simulation replicas[28, 29]. To be able to sample efficiently highly dimensional collective-variable spaces is particularly important in studies of proteins and nucleic acids, as one or two descriptors are often insufficient to adequately to characterize their complex conformational mechanisms [30, 31].

The challenge ahead is thus to formulate a unified approach to derive multidimensional free energy landscapes from an arbitrary number of MD trajectories computed with different adaptive-biasing schemes and defined for multiple CVs. In previous applications, we and others have tackled this problem using the Weighted Histogram Analysis Method (WHAM) [32], an approach that has been extensively applied in the context of non-adaptive biased sampling. The underlying concept is that the effect of the biasing potentials can be removed in post-processing by rebalancing the statistical weights assigned to each of the configurations sampled in the trajectories; the corrected unbiased sampling can be then combined to obtain the best estimate of the free energy. For adaptive biasing techniques such as metadynamics, however, the application of WHAM entails a somewhat arbitrary definition of an "effective" biasing potential"[33, 34],

which is evaluated in a different manner depending on the particular biasing scheme adopted. For example, in standard metadynamics this effective potential is considered to be the time-average of the biasing potential after a certain equilibration time[19, 33, 35], while in well-tempered metadynamics it is considered to be equal to the bias potential at the end of the simulation[19, 36]. Although alternative formulations of WHAM that circumvent the definition of an effective bias are conceivable, they are likely to result in significant numerical errors (as they would require iterative determination of large number of shift constants). For similar reasons, it has been not straightforward so far to apply dynamic histogram[37, 38] or transition-based reweighting analysis[39, 40] in the context of adaptive biases.

Building upon the umbrella integration method[41] and variants thereof formulated for analysis of adaptively-biased simulations[42-45], we propose an alternative general approach for the calculation of multidimensional free energy landscapes, based on the calculation of the free energy gradient or mean force. This approach, which we refer to as Force Correction Analysis Method (FCAM), does not require that an effective potential be defined, and is numerically stable. To demonstrate the validity and performance of this methodology, we compare it with existing analysis methods for simulation data derived for multiple examples, ranging from single trajectories of simple molecular systems with enhanced-sampling of one or two CVs, to multiple exchanging replicas exploring two, six and five-dimensional spaces for small peptides and a multi-domain protein respectively.

Theory

Mean forces estimate from multiple time-dependent biased simulations

To introduce the formulation, we assume to have a set CVs, $\boldsymbol{\xi^f}(\boldsymbol{X}) = \left(\xi_1^f(\boldsymbol{X}), \xi_2^f(\boldsymbol{X}), \dots, \xi_N^f(\boldsymbol{X})\right)$, that are functions of the molecular configurations, $\boldsymbol{X}$. Let us define the free energy as a function of those CVs as:

$$F(\boldsymbol{\xi}) = -\frac{1}{\beta} ln\rho_0(\boldsymbol{\xi}) = -\frac{1}{\beta} ln \int exp\,\{-\beta U(\boldsymbol{X})\}\delta\left(\boldsymbol{\xi} - \boldsymbol{\xi^f}(\boldsymbol{X})\right) d\boldsymbol{X} + C \qquad (1)$$

where $\rho_0(\boldsymbol{\xi})$ is the unbiased probability density in the space of the CVs, $U(\boldsymbol{X})$ is the simulation energy function and C is a constant (and $\beta = 1/k_B T$, in which k_B is the Boltzmann constant, T the temperature). The mean force is the negative of the free energy gradient:

$$f_{\xi_i}(\boldsymbol{\xi}) = -\frac{\partial F(\boldsymbol{\xi})}{\partial \xi_i} \qquad (2).$$

For conventional molecular dynamics (MD) simulations, instead of a Dirac delta, probabilities and free energies are typically calculated using a density kernel, $K_h\left(\boldsymbol{\xi} - \boldsymbol{\xi^f}(\boldsymbol{X})\right)$, e.g. a Gaussian function or a simple binning. In general, the density estimator gives rise to smoothed mean forces, whose accuracy in capturing the correct value depends on the kernel shape and bandwidth.

Namely, integrating over degrees of freedom orthogonal to the CVs and using convolution rules the smoothed mean force can be expressed as:

$$f_{\xi_i}(\boldsymbol{\xi}) \cong -\langle \frac{\partial F(\acute{\boldsymbol{\xi}})}{\partial \acute{\xi}_i} \rangle_{\xi} = -\frac{\int \frac{\partial F(\acute{\boldsymbol{\xi}})}{\partial \acute{\xi}_i} \rho_0(\acute{\boldsymbol{\xi}}) K_h(\boldsymbol{\xi} - \acute{\boldsymbol{\xi}}) d\acute{\boldsymbol{\xi}}}{\int \rho_0(\acute{\boldsymbol{\xi}}) K_h(\boldsymbol{\xi} - \acute{\boldsymbol{\xi}}) d\acute{\boldsymbol{\xi}}} = \langle \frac{1}{\beta} \frac{\partial ln K_h(\boldsymbol{\xi} - \acute{\boldsymbol{\xi}})}{\partial \xi_i} \rangle_{\xi} \qquad (3).$$

The notation $\langle ... \rangle_{\xi}$ stands for local average around $\boldsymbol{\xi}$, which can be calculated as a weighted average over the MD simulation frames, with statistical weights provided by the density kernel, $K_h\left(\boldsymbol{\xi} - \acute{\boldsymbol{\xi}}(t)\right)$, where t denotes the simulation time. For the particular case of a Gaussian density kernel, Eq. 3 becomes equivalent to the typical expression obtained through harmonically restrained simulations[46, 47], $f_{\xi_i}(\boldsymbol{\xi}) \cong k_{\xi_i} \langle \xi_i^f(\boldsymbol{X}) - \xi_i \rangle_{\xi}$, where k_{ξ_i} is the force constant on ξ_i. The latter expression means that in a truly restrained simulation the mean forces are counterbalanced by the harmonic forces. In particular, the presence of restraints directly ensures a locally confined sampling without the need to rebalance the statistical weights of the simulation frames according to the density kernel. Hence, in contrast to unrestrained simulations, the term $\langle ... \rangle_{\xi}$ translates into a simple time average along the simulated trajectory (with equal weight on each frame). However, for standard MD simulations, calculating mean forces through Eq. 3 and integrating them (based on Eq. 2), does not provide any practical advantage over evaluating directly the probability density using Eq. 1. By contrast, mean forces evaluations are particularly convenient for obtaining free energies from multiple biased simulation, as we describe below.

Let us consider the case of a set of simulation replicas, each denoted with the index *r*, and on which a time-dependent bias potential, $V_r(\boldsymbol{\xi}, t)$**,** is applied, which may entail a different biasing scheme (e.g. standard or well-tempered metadynamics[19, 48]) or act on different subsets of the CVs depending on the trajectory (as in bias exchange metaynamics[28]). Additionally, as expected for properly set metadynamics[17-19] or ABF simulations[14-16], we assume a slow time variation of $V_r(\boldsymbol{\xi}, t)$ such that the simulations can be considered constantly at equilibrium.

In the WHAM[32] based approach that we used in our previous studies[33, 34, 49-51], the unbiased probability density, $\rho_0^r(\boldsymbol{\xi})$, for trajectory *r*, was obtained based on umbrella sampling re-weighting[13, 32] according to an effective bias potential, $\bar{V}_r(\boldsymbol{\xi})$, namely, by adjusting the statistical weight of each simulation frame, $\acute{t}$, as:

$$\rho_0^r(\boldsymbol{\xi}) \cong \sum_{\acute{t}} exp\left\{\beta \bar{V}_r\left(\boldsymbol{\xi}(\boldsymbol{X}_{\acute{t}}^r)\right) - f_r\right\} K_h\left(\boldsymbol{\xi} - \boldsymbol{\xi}^f(\boldsymbol{X}_{\acute{t}}^r)\right) \qquad (4).$$

In which $\boldsymbol{X}_{\acute{t}}^r$ is the molecular conformation of trajectory *r* at time $\acute{t}$, f_r is a shift constant evaluated iteratively. The kernel $K_h\left(\boldsymbol{\xi} - \boldsymbol{\xi}^f(\boldsymbol{X}_{\acute{t}}^r)\right)$ was typically selected as a simple binning ($K_h\left(\boldsymbol{\xi} - \boldsymbol{\xi}^f(\boldsymbol{X}_{\acute{t}}^r)\right) = 1$ if $\boldsymbol{\xi}^f(\boldsymbol{X}_{\acute{t}}^r)$ belongs to a bin centered in $\boldsymbol{\xi}$ and is zero otherwise). The final free energies are determined by combining the unbiased probabilities from all trajectories:

$$F(\boldsymbol{\xi}) \cong -\frac{1}{\beta} ln\left(\sum_r \pi^r(\boldsymbol{\xi})\, \rho_0^r(\boldsymbol{\xi})\right) + C \qquad (5),$$

in which the terms $\pi^r(\boldsymbol{\xi})$ ensure a minimal error on the free energy (according to Poisson's statistics). Despite WHAM provides a rigorous framework for combining the sampling of multiple trajectories, owing to the time-dependent nature of the bias, there is no uniform procedure for the definition of the effective potentials, $\bar{V}_r(\boldsymbol{\xi})$, across multiple adaptive biasing schemes. For example, in standard metadynamics $\bar{V}_r(\boldsymbol{\xi}) = (t_{tot} - t_F)^{-1} \int_{t_F}^{t_{tot}} V_r(\boldsymbol{\xi}, t) dt$[19, 33, 35] while in well-tempered metadynamics $\bar{V}_r(\boldsymbol{\xi}) = V_r(\boldsymbol{\xi}, t_{tot})$[19, 36, 51, 52], where t_{tot} is the total simulation time and t_F (filling time) is an equilibration time after which the bias potential can be considered approximately stationary. A strategy to avoid resorting to effective biasing potentials would be to use directly the instantaneous bias potential, $V_r(\boldsymbol{\xi}, t)$, and apply Eq. 4 for small simulation intervals, Δt, e.g. at any bias potential update. Nonetheless, this would imply a different additive constant, f_r, for each bias potential update, thus leading to a large number of shift constants that must be iteratively determined.

Hereafter, we derive an alternative general approach based on the evaluation of the mean force, that does not require the definition of an effective potential nor the iterative evaluation of additive constants. Let us apply Eq. 1, through the density kernel $K_h\left(\boldsymbol{\xi} - \boldsymbol{\xi}^{\boldsymbol{f}}(\boldsymbol{X})\right)$, on a time interval, Δt, of trajectory *r*, that is short enough so that the time dependence of the bias potential can be neglected. Owing to the presence of $V_r(\boldsymbol{\xi}, t)$, this operation will generally produce a biased estimate of the free energy:

$$\begin{aligned} F_b^r(\boldsymbol{\xi}, t, \Delta t) &= -\frac{1}{\beta} ln \sum_{\acute{t}=t-\Delta t/2}^{t+\Delta t/2} K_h\left(\boldsymbol{\xi} - \boldsymbol{\xi}^{\boldsymbol{f}}\left(\boldsymbol{X}_{\acute{t}}^r\right)\right) \\ &\cong -\frac{1}{\beta} ln \int exp\left\{-\beta\left(U(\boldsymbol{X}) + V_r\left(\boldsymbol{\xi}^{\boldsymbol{f}}(\boldsymbol{X}), t\right)\right)\right\} K_h\left(\boldsymbol{\xi} - \boldsymbol{\xi}^{\boldsymbol{f}}(\boldsymbol{X})\right) d\boldsymbol{X} \\ &+ C \end{aligned} \quad (6).$$

In which the right-hand side of Eq. 6 arises from the equilibrium assumption[13, 41]. To relate Eq. 6 to the unbiased free energy is convenient to integrate over the degrees of freedom orthogonal to the CVs: $F_b^r(\boldsymbol{\xi}, t, \Delta t) \cong -\beta^{-1} ln \int exp\left\{-\beta\left(F(\acute{\boldsymbol{\xi}}) + V_r(\acute{\boldsymbol{\xi}}, t)\right)\right\} K_h(\boldsymbol{\xi} - \acute{\boldsymbol{\xi}}) d\acute{\boldsymbol{\xi}} + C$. Taking the derivatives of latter expression (and using convolutions rules), we obtain that the unbiased mean force, $f_{\xi_i}^r(\boldsymbol{\xi}^{\boldsymbol{c}}, t, \Delta t)$, can be recovered from the biased one by simply subtracting the local average of the forces arising from the bias potential:

$$f_{\xi_i}^r(\boldsymbol{\xi}, t, \Delta t) \cong \frac{\sum_{\acute{t}=t-\Delta t/2}^{t+\Delta t/2}\left(\frac{1}{\beta}\frac{\partial ln K_h\left(\boldsymbol{\xi} - \boldsymbol{\xi}^{\boldsymbol{f}}\left(\boldsymbol{X}_{\acute{t}}^r\right)\right)}{\partial \xi_i} + \left(\frac{\partial V_r(\acute{\boldsymbol{\xi}}, \acute{t})}{\partial \acute{\xi}_i}\right)_{\acute{\boldsymbol{\xi}}=\boldsymbol{\xi}^{\boldsymbol{f}}\left(\boldsymbol{X}_{\acute{t}}^r\right)}\right) K_h\left(\boldsymbol{\xi} - \boldsymbol{\xi}^{\boldsymbol{f}}\left(\boldsymbol{X}_{\acute{t}}^r\right)\right)}{\sum_{\acute{t}=t-\Delta t/2}^{t+\Delta t/2} K_h\left(\boldsymbol{\xi} - \boldsymbol{\xi}^{\boldsymbol{f}}\left(\boldsymbol{X}_{\acute{t}}^r\right)\right)} \quad (7)$$

A general expression of the mean force can now be obtained as the weighted average[41] of all the unbiased estimates, $f_{\xi_i}^r(\boldsymbol{\xi^c}, t, \Delta t)$, obtained for all time intervals and simulations trajectories, according to the weights, $\sum_{\acute{t}=t-\Delta t/2}^{t+\Delta t/2} K_h\left(\boldsymbol{\xi} - \boldsymbol{\xi^f}\left(\boldsymbol{X}_{\acute{t}}^r\right)\right)$:

$$f_{\xi_i}(\boldsymbol{\xi}) \cong \frac{\sum_r \sum_t \left(\frac{1}{\beta}\frac{\partial lnK_h\left(\boldsymbol{\xi} - \boldsymbol{\xi^f}(\boldsymbol{X}_t^r)\right)}{\partial \xi_i} + \left(\frac{\partial V_r(\acute{\boldsymbol{\xi}}, t)}{\partial \acute{\xi}_i}\right)_{\acute{\boldsymbol{\xi}}=\boldsymbol{\xi^f}(\boldsymbol{X}_t^r)}\right) K_h\left(\boldsymbol{\xi} - \boldsymbol{\xi^f}(\boldsymbol{X}_t^r)\right)}{\sum_r \sum_t K_h\left(\boldsymbol{\xi} - \boldsymbol{\xi^f}(\boldsymbol{X}_t^r)\right)} \quad (8)$$

$$= \langle \frac{1}{\beta}\frac{\partial lnK_h\left(\boldsymbol{\xi} - \boldsymbol{\xi^f}(\boldsymbol{X}_t^r)\right)}{\partial \xi_i} \rangle_{\xi} + \langle \left(\frac{\partial V_r(\acute{\boldsymbol{\xi}}, t)}{\partial \acute{\xi}_i}\right)_{\acute{\boldsymbol{\xi}}=\boldsymbol{\xi^f}(\boldsymbol{X}_t^r)} \rangle_{\xi}$$

The general meaning of Eq. 8 is that the mean force is the result of the total force inferred from the combined probability density of all simulation trajectories, corrected by subtracting the local average across all trajectories, $\langle \ldots \rangle_{\xi}$, of the instantaneous forces originating from the different biasing potentials applied. Note that in contrast to WHAM (Eq. 4), Eq. 8 does not entail effective biasing potentials nor additive constants that must be iteratively evaluated. Hence, it provides a more general formulation valid for any type and combination of adaptively-biased simulations, provided they fulfill the quasi-equilibrium assumption. For metadynamics and ABF approaches, equilibrium conditions are more easily fulfilled after the simulation has explored the relevant regions of the CVs space, so that there are no large trajectory drifts and the forces of the bias potential oscillate around well-defined values.

As in Eq. 3, the effect of the density kernel is to produce a smoothing of the mean forces, hence, a specific selection and tuning of the latter kernel may become particularly advantageous for accurate high dimensional analysis[30]. In all the applications presented in this work, mean forces were calculated according to a simple density kernel selected as a product of Gaussians (with standard deviations $\sigma_{\xi_i} = \sqrt{k_B T / k_{\xi_i}}$), for which Eq. 8 becomes:

$$f_{\xi_i}(\boldsymbol{\xi}) \cong \frac{\sum_r \sum_t w_t^r(\boldsymbol{\xi}) \left[k_{\xi_i}\left(\xi_i^f(\boldsymbol{X_t^r}) - \xi_i\right) + \left(\frac{\partial V_r(\acute{\boldsymbol{\xi}}, t)}{\partial \acute{\xi}_i}\right)_{\acute{\boldsymbol{\xi}}=\boldsymbol{\xi^f}(\boldsymbol{X}_t^r)}\right]}{\sum_r \sum_t w_t^r(\boldsymbol{\xi})} \quad (9),$$

where $w_t^r(\boldsymbol{\xi}) = exp\left\{-\sum_{i=1}^N k_{\xi_i}\left(\xi_i^f(\boldsymbol{X_t^r}) - \xi_i\right)^2 / 2k_B T\right\}$, in which the terms k_{ξ_i} can be considered as smoothing parameters that must be selected large enough so as to capture the relevant features of the underlying free energy. Note that for a single trajectory or type of bias potential, and assuming that within a small region around $\boldsymbol{\xi}$, $\left(\partial V_r(\acute{\boldsymbol{\xi}}, t)/\partial \acute{\xi}_i\right)_{\acute{\boldsymbol{\xi}}=\boldsymbol{\xi^f}(\boldsymbol{X_t^r})} \approx \left(\partial V_r(\acute{\boldsymbol{\xi}}, t)/\partial \acute{\xi}_i\right)_{\acute{\boldsymbol{\xi}}=\boldsymbol{\xi}}$, Eq. 9 becomes equivalent to the expression derived by Marinova & Salvalaglio in the context of metaydnamics simulations[45]. The latter condition results in different smoothing for contributions arising from biased probability density and bias potential, and provides a reasonable

alternative for analyzing metadynamics trajectories, as in the latter the biased probability density becomes gradually uniform. An advantage of Eq. 8 or 9 is that they require only the instantaneous value of the biasing force, $\left(\partial V_r(\acute{\boldsymbol{\xi}}, t)/\partial \acute{\xi}_i\right)_{\acute{\xi}=\xi^f(\boldsymbol{X}_t^r)}$, that can be easily calculated or made directly available by current enhanced sampling simulation programs[53-57].

As the mean force given by Eq. 8-9 arises from a local average, error estimates can be achieved through block averages or autocorrelation analysis[16]. Assuming the same autocorrelation time for all trajectories and time intervals, the statistical error would be proportional to $\left(\sqrt{\sum_r \sum_t K_h\left(\boldsymbol{\xi} - \xi^f(\boldsymbol{X}_t^r)\right)}\right)^{-1}$, where the sum of the weights is associated to the number of effective frames around $\boldsymbol{\xi}$.

It is worth pointing out that mean forces can be alternatively evaluated using the same formulation adopted in the ABF approach, namely as a local average, around $\boldsymbol{\xi}$, of the instantaneous forces arising from the simulation energy function, $U(\boldsymbol{X})$, and effectively projected along the CVs[14-16, 58-60]. Assuming equilibrium condition, such local average would not be affected by any bias potential that depends only on the CVs[56], hence it could be in principle applied in the context multiple trajectories and biases. This notwithstanding, implementation difficulties and/or inapplicability in presence of constraints and multiple related CVs[16], has made this analysis unavailable for several types of CVs and simulation programs. Here, we use the latter mean force estimate for comparative analysis with the proposed approach across simple mono and two-dimensional examples (see applications to butyramide and deca-L-alanine). In particular, we used the implementation available in NAMD[61, 62] through the Colvars module[56], from which mean forces are derived as[60]:

$$f_{\xi_i}(\boldsymbol{\xi}) = \langle -\nabla U \cdot v_i + \frac{1}{\beta} \nabla \cdot v_i \rangle_{\boldsymbol{\xi}} \qquad (10),$$

in which the term $-\nabla U$ denotes the atomic forces and v_i is a vector field satisfying a set of orthonormality/orthogonality conditions: $v_i \cdot \nabla \xi_j = \delta_{ij}$ and $v_i \cdot \nabla \sigma_k = 0$, where $\sigma_k(\boldsymbol{X}) = 0$ defines a constraint applied to the simulation.

Multidimensional free energy landscapes from mean forces

After evaluating the mean forces on a dense set of CVs configurations $(\xi_1^\alpha, \xi_2^\alpha, \dots, \xi_N^\alpha)$, e.g. placed on a regular grid, the free energy can be calculated according to Eq. 2 by mean forces integration[47]. To do this accurately and efficiently across multiple dimensions, we adopted a kinetic Monte Carlo (KMC) approach. The KMC simulations are based on a transition rate between neighboring bins, α and β, that satisfies the detailed balance[33]:

$$R_{\alpha\beta} = \left(\tau_{\alpha\beta}^0\right)^{-1} exp\left\{-\beta \frac{\Delta F_{\alpha\beta}}{2}\right\} \qquad (11).$$

Assuming the transitions dynamics between bins is well approximated by the Markovian model described by Eq. 11, the latter can be also used to obtain kinetic information, provided $\left(\tau_{\alpha\beta}^0\right)^{-1}$

reflects the diffusion rate[33]. The main purpose of this work, however, is to obtain an accurate evaluation of the free energy, which is invariant under changes of $\tau^0_{\alpha\beta}$, hence, here we arbitrarily set the preexponential term as a geometric factor: $\tau^0_{\alpha\beta} = \sum_{i=1}^{N}\left(\left(\xi_i^\beta - \xi_i^\alpha\right)/\Delta\xi_i\right)^2$, where $\Delta\xi_i$ are the bin widths of the grid. The free energy difference between α and β, $\Delta F_{\alpha\beta} = F(\boldsymbol{\xi^\beta}) - F(\boldsymbol{\xi^\alpha})$, is obtained from the mean forces using finite differences:

$$\Delta F_{\alpha\beta} = -\sum_i \frac{\left(f_{\xi_i}(\boldsymbol{\xi^\alpha})w(\boldsymbol{\xi^\alpha}) + f_{\xi_i}(\boldsymbol{\xi^\beta})w(\boldsymbol{\xi^\beta})\right)}{w(\boldsymbol{\xi^\alpha}) + w(\boldsymbol{\xi^\beta})}\left(\xi_i^\beta - \xi_i^\alpha\right) \qquad (12),$$

where $w(\boldsymbol{\xi^{\alpha/\beta}}) = \sum_r \sum_t w_t^r(\boldsymbol{\xi^{\alpha/\beta}})$ are the total weights of each of the two bins (see Eq. 9).
Finally, the free energies can be estimated as in Eq. 1 using the bin probabilities calculated over a long KMC trajectory, $F(\boldsymbol{\xi^\alpha}) = -\beta^{-1} ln\left[\left(N_\alpha^{KMC}/\sum_\beta R_{\alpha\beta}\right)\left(\sum_\alpha N_\alpha^{KMC}/\sum_\beta R_{\alpha\beta}\right)^{-1}\right]$, where N_α^{KMC} is the number of times the KMC trajectory visits bin α.
The advantage of using KMC simulations is that, once neighboring bins are assigned, the interconnected regions of the CVs space are automatically identified during the KMC trajectory. Furthermore, statistical convergence can be easily achieved as running long KMC simulations (for billion steps) is not computationally demanding and eventually they can be carried out at raised temperature to efficiently cross free energy barriers.

Ensemble reweighting from free energy analysis

The unbiased distribution from the sampling of all trajectories can be easily recovered considering that the biasing potentials depend only on the CVs, hence, within a small bin of the latter variables the sampling distribution remains unbiased. This implies that the statistical weight assigned to each configuration, $\Omega(\boldsymbol{X_t^r})$, in order to obtain unbiased sampling, is only a function of the CVs; $\Omega(\boldsymbol{X_t^r}) = \Omega\left(\xi_1^f(\boldsymbol{X_t^r}), \xi_2^f(\boldsymbol{X_t^r}), \dots, \xi_N^f(\boldsymbol{X_t^r})\right)$. An analytical expression for the weight can be derived by imposing that the reweighted ensemble conforms to the calculated free energy:

$$\Omega(\boldsymbol{\xi^\alpha}) = \frac{1}{N_\alpha}\exp\{-\beta F(\boldsymbol{\xi^\alpha})\} \qquad (13).$$

In which N_α is the total number of frames from all trajectories in a bin, α, of the CVs.
This reweighting scheme can be applied to the cumulative sampling of all trajectories to calculate unbiased ensemble averages or to estimate the free energy as a function of different reaction coordinates.

Minimum free energy paths calculation across multidimensional landscapes

The minimum free energy path between two configurations, α_1, α_N, of the CVs space reflects the most probable pathway observed at vanishing temperature[63]. Assuming this pathway arises from a set of stochastic transitions between CVs space bins, the minimum free energy path is defined by the set of transitions that maximizes the time-independent probability of a stochastic path

connecting the two endpoints and evaluated at nearly zero temperature[63, 64]. The latter path probability is given by the product of the normalized pairwise transition probabilities between the associated bins, which can be derived according to the KMC rates reported in Eq. 11 [49, 64]:

$$P^{KMC}_{\alpha_1,\alpha_N} = P^{KMC}_{\alpha_1,\alpha_2} P^{KMC}_{\alpha_2,\alpha_3} \dots, P^{KMC}_{\alpha_{N-1},\alpha_N} \quad (14).$$

In which $P^{KMC}_{\alpha_i,\alpha_j} = R_{\alpha_i,\alpha_j} / \sum_{\alpha_j} R_{\alpha_i,\alpha_j}$ is the probability to observe a transition between α_i and α_j. In this case the rates of Eq. 11, R_{α_i,α_j}, are evaluated using a very low temperature, in which we consider that the approximation of a preexponential factor evaluated by a geometric term instead of a diffusion rate[33] is sufficient to identify a most likely pathway. The minimum free energy pathways reported in this work were obtained using first a global search with KMC trajectories and then a refinement step in which new pathways are generated by randomly selecting two intermediate configurations along the current pathway and running a KMC trajectory that connects them. The sampled pathways are accepted or rejected according to a Monte Carlo (MC) scheme that samples the distribution $exp\{-log(P^{KMC}_{\alpha_1,\alpha_N})/T_{MC}\}$, in which T_{MC} represents a dimensionless temperature factor. Different MC runs are carried out by gradually reducing T_{MC} using a simulated annealing protocol in order to converge to the most probable pathway.

Computational details

Metadynamics simulations of solvated butyramide and deca-L-alanine were carried out at 298 K with NAMD versions 2.12-2.14[61, 62] and colvars[56], using the CHARMM27/CMAP force field[65, 66]. Simulations of butyramide were performed at constant pressure (1 bar), with 1-fs time step and periodic boundary conditions. The molecular system comprises butyramide in a cubic box with 1467 water molecules. Simulations of deca-L-alanine were carried out in gas phase, with 0.5 fs time step[15]. To permit the correct evaluation of instantaneous forces according to Eq. 10, no constraints were used on the chemical bonds of butyramide and deca-L-alanine [16]. Short-range electrostatic and van der Waals interactions were calculated with Coulomb and Lennard-Jones potentials, respectively, with a cut off at 12 Å. For simulations of butyramide, long-range electrostatic interactions were calculated with the particle-mesh Ewald (PME) method. In this system, metadynamics bias potentials were constructed adding Gaussians of widths 5° and 10° for standard and concurrent metadynamics, respectively. In the case of deca-L-alanine, the Gaussians width was set to 0.5 Å. Gaussians were added every 1 ps and 0.5 ps for butyramide and deca-L-alanine systems respectively. Multiple sets of simulations were carried out at different values of the Gaussian height, ranging from 0.025 to 5 kcal/mol for the butyramide simulation system and 0.005 to 0.5 kcal/mol for deca-L-alanine (Fig. 3 and Fig. 5). For the latter system, reflective conditions of the bias potential and confinement quadratic restraints were applied at the boundaries (11 and 32 Å) to ensure that stationary conditions are reached[67]. The bias-exchange metadynamics simulations[28] of alanine dipeptide and Ace-Ala_3-Nme peptide were carried out at 298 K and 1 bar with GROMACS 4.5.5/PLUMED[53, 55, 68] (and time step of 2 fs), Short-range electrostatic and van der Waals interactions were cut off at 9 Å; long-range electrostatic

interactions were calculated with PME. In this case, the metadynamics bias potential was constructed using Gaussians of height 0.024 kcal/mol and width 5.7°, added every 2 ps. Exchanges between replicas were attempted every 2 ps. The alanine dipeptide simulation used the CHARMM27 force field[65], and includes 877 water molecules enclosed in a periodic cubic box. The simulations of the Ace-Ala_3-Nme peptide used the AMBER03 force field[69] and include 1052 water molecules in a periodic cubic box. Computational details for the simulations of the SH3-SH2 tandem of the Abl kinase have been reported elsewhere[50]. Statistics for the calculation of mean forces was collected every simulation step for simulations of butyramide and deca-L-alanine, every 100 steps for alanine dipeptide and Ace-Ala_3-Nme peptide, and every 250 steps for ABL kinase.

Results and Discussion

FCAM converges rapidly and accurately in one-dimensional test case

To evaluate the accuracy and convergence rate of the proposed approach, we first considered as a 'gold standard' a simple molecular process for which mean forces and free energies can be derived readily with existing methods, namely the isomerization of solvated butyramide. Ten independent metadynamics simulations[17-19] were carried out using the Φ dihedral angle as CV (Fig. 1). In this approach a time-dependent bias potential is constructed as a sum of Gaussians centered on the values of Φ visited during the trajectory. Over time, this bias potential results in uniform sampling of Φ by gradually compensating the underlying free energy. Thus, after an equilibration time the bias potential oscillates around the negative of the free energy profile along Φ [17-19]; this so-called 'filling time' is ~6 ns in this case. For each trajectory, we calculated the mean forces as a function of the value of Φ (in increments of 1°) using either the FCAM method (Eq. 9) or by computing the local average of the instantaneous forces[15], which for dihedral angles can be evaluated analytically (Eq. 10). (For consistency, the latter average, evaluated similarly to Eq. 3, was calculated using the same Gaussian density estimator adopted for estimates obtained through Eq. 9, with the Gaussian standard deviation set to 1°.) In addition, we calculated free energy and mean forces with an umbrella-sampling (US) simulation of 140 ns, using a static bias potential, $V_{US}(\Phi)$ (derived from a 20-ns metadynamics simulation). In this case, the free energy was estimated using standard histogram reweighting[13]: $F_{US}(\Phi) = -\beta^{-1} ln(\rho_{US}(\Phi) exp\{\beta V_{US}(\Phi)\})$, where $\rho_{US}(\Phi)$ is the histogram along Φ obtained from the US simulation (using a binning width of 1°). The associated mean forces were obtained by finite differences from $F_{US}(\Phi)$.

Fig. 1AB highlights how mean force and free energy profiles (obtained from mean forces integration) calculated from the combined sampling of all metadynamics trajectories (300 ns in Fig. 1AB) and estimated either with Eq. 9 (FCAM in Fig. 1) or Eq. 10 (MIF and MIF-I in Fig. 1), perfectly match the US results. Specifically, regardless of the type of estimate, the mean discrepancy with respect to the US profiles is in the same order of magnitude of the statistical error on the latter, which is on average 0.002 kcal/(mol deg) and 0.01 kcal/mol for mean force and free

energy estimates respectively (evaluated through block averages). For this simple system, estimates derived from the proposed approach converge after a few ns (Fig. 1), before the metadynamics bias potential reaches a stationary condition (filling time in Fig. 1D). Importantly, the time dependence of the error (with respect to US estimates) on mean forces and free energy (Fig. 1CD) highlights how, for this example, the proposed approach achieves the same convergence rate and accuracy of estimates obtained thorough mean instantaneous forces (MIF and MIF-I in Fig. 1CD; evaluated according to Eq. 10). Conversely, the free energy profile directly inferred from the time average of the metadyamics bias potential after the filling time[33, 35] (purple line in Fig. 1D) is directly dependent on the parameters used to construct the bias (Gaussian height and widths) and in this case is less accurate than mean forces-based estimates. The same accuracy of the latter can be instead achieved by introducing US corrections to the mean bias potential estimate[33] (through Eq. 4; blue line in Fig. 1D), which nevertheless can be evaluated only after the filling time.

Once an accurate estimate of the free energy along Φ is obtained, an unbiased ensemble can be recovered using the reweighting scheme provided by Eq. 13. For example, this procedure can be used to calculate the unbiased free energy along the Ψ dihedral angle (structural drawing in Fig. 1), even though sampling of this angle was not directly enhanced. As shown in Fig. 2, this free energy profile perfectly matches the one resulting from a 400 ns MD simulation generated without any bias [67], demonstrating that this procedure is highly accurate.

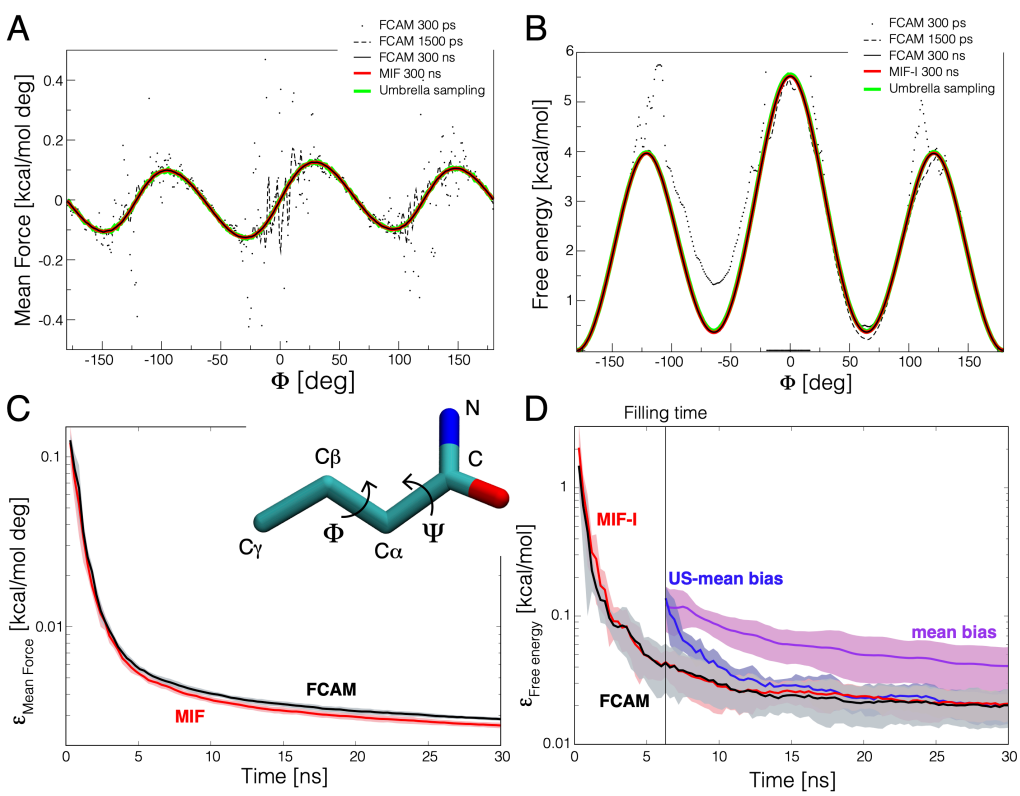

Figure 1. Benchmark test of the proposed approach on metadynamics simulations along the Φ dihedral angle of solvated butyramide. The latter molecule and its Φ and Ψ dihedral angles are illustrated in the figure. The

metadynamics bias potential was constructed using Gaussians of height 0.025 kcal/mol. (A, B) Comparison between mean forces (panel A) and free energies (panel B) calculated using Eq. 9 (FCAM at different time intervals), Eq. 10 (MIF and MIF-I; the notation -I denotes integration)[15] and 140 ns umbrella sampling (US) simulation[13] (green line). Mean forces from US were calculated using finite differences from the free energy profile. (C, D) Root mean square deviation of mean forces and free energies with respect to US reference values, evaluated over grid points, Φ_i: $\varepsilon_O = \sqrt{\sum_{i=1}^{N}\left(O(\Phi_i) - O_{US}(\Phi_i)\right)^2/N}$, where $O = Mean\ Force\ or\ Free\ energy$ and O_{US} is the US reference value. The purple line in panel D is the error (ε_O) of the free energy calculated as the time average of the bias potential after the filling time[19, 33, 35].The blue line on the same panel is error obtained by including US corrections on the previous estimate (Eq. 4)[33]. Lines and shaded regions reflect average error and standard deviations, respectively, arising from 10 independent metadynamics trajectories.

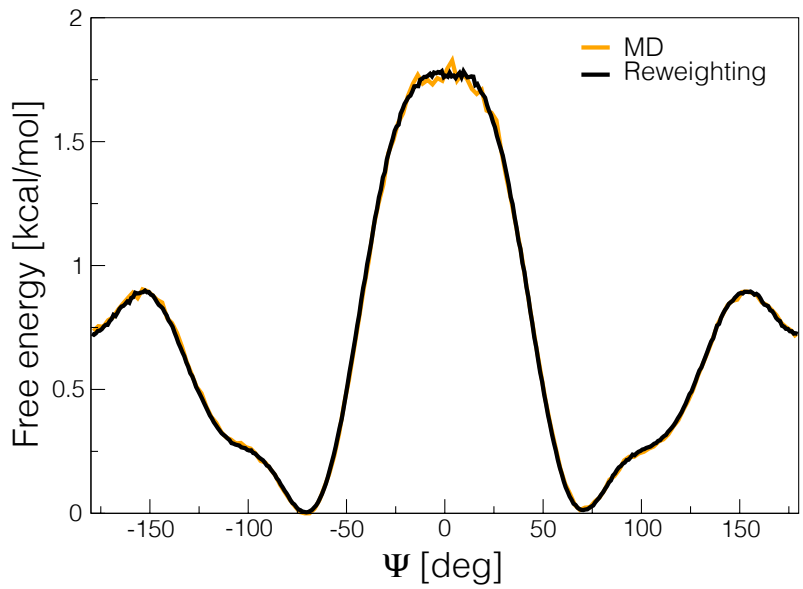

Figure 2. Free energy along the Ψ dihedral angle of butyramide obtained through 400 ns MD simulation (orange line) and ensemble reweighting using Eq. 13. The reweighting was carried out on the combined sampling of 10 metadynamics simulations using the Φ dihedral angle as CV. The free energies used in Eq. 13 were derived from the same simulations using FCAM (Eq. 9 and mean forces integration).

To assess the effect of the amplitude of the time-fluctuations of the bias potential on free energy and mean force estimates, we performed analogous sets of simulations using different values of the Gaussians height for constructing the metadynamics bias potential. By gradually raising the latter height (w) from 0.025 to 5 kcal/mol, the time-fluctuations of the bias potential become larger and larger [70, 71], (Fig. S1), with an average standard deviation that increases from 0.1 to 4.6 kcal/mol. For this system and inspected ranges, regardless of the type of estimate used, the final accuracy of mean forces and free energies is rather insensitive to the amplitude of the bias potential fluctuations (Fig. 3AB). These results are consonant with the fast equilibration times of this simple test system. Increasing the value of the Gaussians height also leads to reduced filling times (see above) and consequently a faster exploration of the space of the biased Φ dihedral angle. Hence, up to moderate Gaussian height (below 0.5 kcal/mol), larger values of this parameter induce a more rapid convergence of mean forces and free energies (Fig. 3CD). A slight accuracy loss is only detected at the largest inspected value of the Gaussians height (w=5 kcal/mol, Fig. 3CD), for

which the time-fluctuations of the bias potential reach the same order of magnitude of the free energy changes along Φ, while the average bias potential still resembles the underlying free energy (Fig. S1). Such accuracy deterioration is more pronounced for the FCAM methodology for which mean forces estimates are directly dependent on the biasing forces (Eq. 8-9). Nonetheless, for such large fluctuations of the bias potential, a marginal loss in accuracy is also present for estimates based on Eq. 10 (Fig. 3CD), thus denoting the onset of systematic errors associated to lack of equilibration in the degrees of freedom orthogonal to the biased Φ dihedral angle (as Eq. 10 reflects an average over the latter degrees of freedom[16] and does not depend directly on the bias potential).

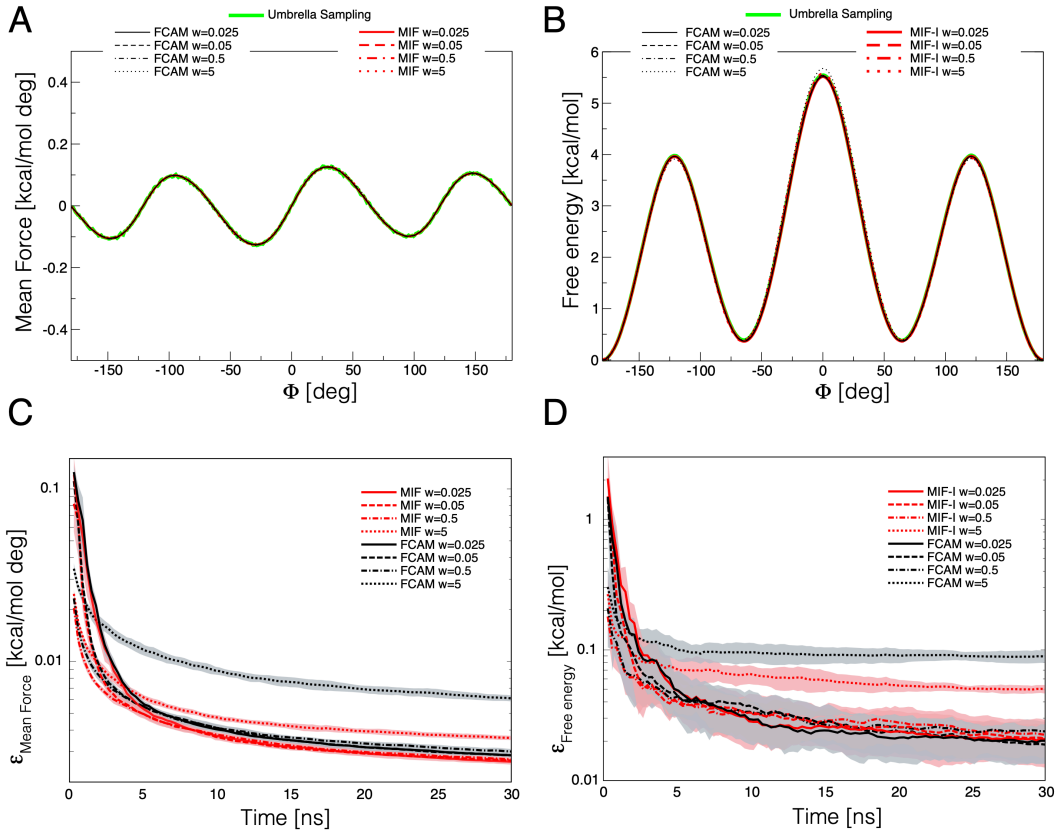

Figure 3. Effect of the bias potential time-fluctuations on accuracy and convergence rate of mean forces and free energies calculated from a one-dimensional metadynasmics simulations of solvated butyramide. (A, B) Mean forces and free energy profiles estimated with FCAM (black lines) and Eq. 10 (red lines) at different values of the Gaussians height (w) for constructing the metadynamics pontential. Every profile is calculated from the combined sampling of 10 independent metadynamics trajectories of 30 ns each. The latter profiles are compared with the one obtained with umbrella sampling (green line; same as Fig. 1). (C, D) Time dependence of the average discrepancy respect to umbrella sampling estimates (see Fig. 1 caption) of mean forces and free energies calculated using FCAM (black lines) and Eq. 10 (red lines) at different values of w. Lines and shaded regions reflect the average discrepancies and their standard deviations respectively, calculated as in Fig. 1 (see associated caption).

FCAM converges rapidly and accurately in deca-L-alanine unfolding test case

To verify whether FCAM retains similar accuracy and convergence properties on a different system and type of CV, we assessed the performance of this approach for calculating the free

energy of reversible unfolding of the deca-L-alanine; a benchmark test system for free energy methods[15, 16, 60, 72]. As for the butyramide system, we performed ten independent metadynamics simulations (of 100 ns each) biasing in this case the end-to-end distance of the peptide (distance between the carbon atoms of carbonyl groups of residues 1 and 10), so as to enable the reversible simulation of folding/unfolding transitions, i.e. from α-helical (below 16 Å in Fig. 4B) to extended conformations (beyond 16 Å in Fig. 4B). Fig. 4AB outlines how also for this system, mean forces and free energies calculated using either FCAM (Eq. 9) or mean instantaneous forces (Eq. 10)[15] (using bin width and standard deviation of the Gaussian density estimator of 0.1 Å), closely resemble the profiles derived in previous studies[15, 16, 60, 72] and perfectly match (within the uncertainty) the reference values obtained through US simulations. The average statistical error in the latter calculations (obtained through blocks analysis) is 0.05 kcal/(mol Å) and 0.1 kcal/mol for mean forces (derived from finite differences) and free energies (derived as for butyramide) respectively. The US simulations entail a static bias potential derived from previous multiple walkers metadynamics[73] simulations (500 ns sampling, using 10 walkers) and comprise 10 independent simulation replicas of 100ns each.

Remarkably, the convergence rate of the average error in mean forces and free energy (with respect to US values) is almost identical between estimates based on FCAM and mean instantaneous forces (Eq. 10, Fig. 4CD). Owing to the large free energy difference between folded and extended conformations, a reasonable accuracy in mean forces and free energies profiles can be achieved only near or after the filling time, when the full range of the end-to-end distances becomes energetically feasible (Fig. 4). For this application and choice of the metadynamics parameters (Gaussian height and width), the free energy derived from the mean bias potential after the filling time (~20 ns) reaches similar accuracy of corresponding estimates based on FCAM or mean instantaneous forces (Eq. 10). Furthermore, US corrections do not lead in this case to improvements in the accuracy (Fig. 4D).

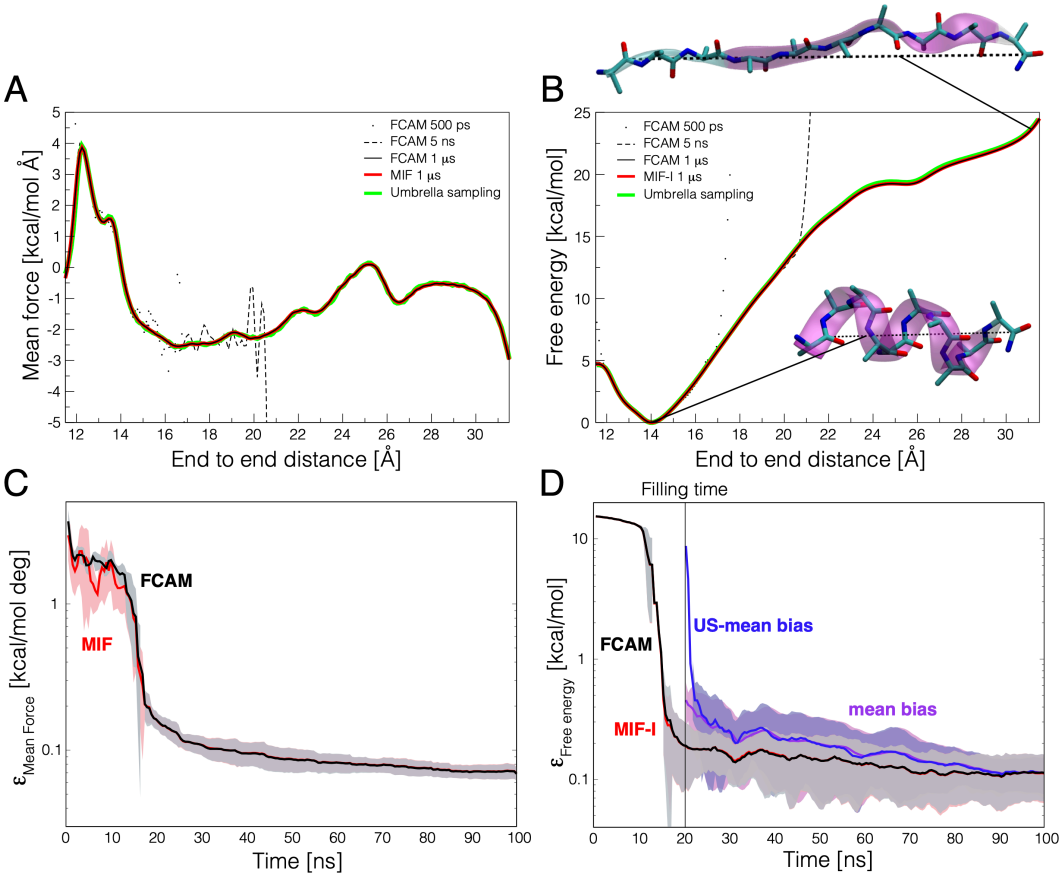

Figure 4. Assessment of the performance of FCAM on metadynamics simulations of deca-L-alanine biased along the end-to-end distance. (A, B) Comparison between the mean forces (panel A) and free energies (panel B) calculated using FCAM (shown for different time intervals), the mean instantaneous forces (MIF and MIF-I; based on Eq. 10)[15] and 1 μs US simulation[13] (profiles in green). In either case 1 μs sampling arises from 10 independent simulations of 100 ns each. (C, D) Time dependence of the average deviation with respect to US estimates (evaluated as reported in the caption of Fig. 1) of the mean forces calculated using FCAM and MIF (panel C) and the free energies using different types of estimates (panel D). The purple line in panel D reflects the error on the free energy estimated as the time average of the bias potential after the filling time[19, 33, 35].The blue line represent the free energy error by including US corrections to the estimate based on the mean bias potential (as in Eq. 4)[33]. Lines and shaded regions in panels C and D reflect average error and standard deviations respectively, evaluated over 10 independent metadynamics trajectories.

For this application we also evaluated the effect of the time-fluctuations of the metadynamics bias potential on accuracy and convergence rate of mean forces and free energies. To this end, we performed additional metadynamics simulations with Gaussian height (w) ranging from 0.005 to 0.5 kcal/mol, leading to bias potential fluctuations (measured in terms of standard deviation) that go from 0.5 to 5 kcal/mol (Fig. S2). The results outline that, regardless of the value of the Gaussian height, FCAM (Eq. 9) and mean instantaneous forces (Eq. 10) feature nearly identical accuracy and convergence rate (Fig. 5). Nonetheless, in contrast to the butyramide case, by increasing the value of w either of the two estimates diverge more and more from the correct free energy profile, represented by the one calculated with US (Fig. 5). These systematic errors arise from slow degrees of freedom in directions orthogonal to end-to-end distance, which cannot reach full equilibration in presence of large time-oscillations of the bias potential. Such error is more pronounced at large

values of the latter CV (Fig. 5 and Fig. S2), which comprise a heterogeneous ensemble of slowly interconverting extended conformations. Other than decreasing the time-fluctuations of the bias potential, an effective strategy to reduce this type of errors, is to construct an optimal CV that includes all the slowest degrees of freedom, for example by using spectral gap analysis[23]. Another possibility is to bias many CVs simultaneously, which altogether encompass all the slow degrees of freedom.

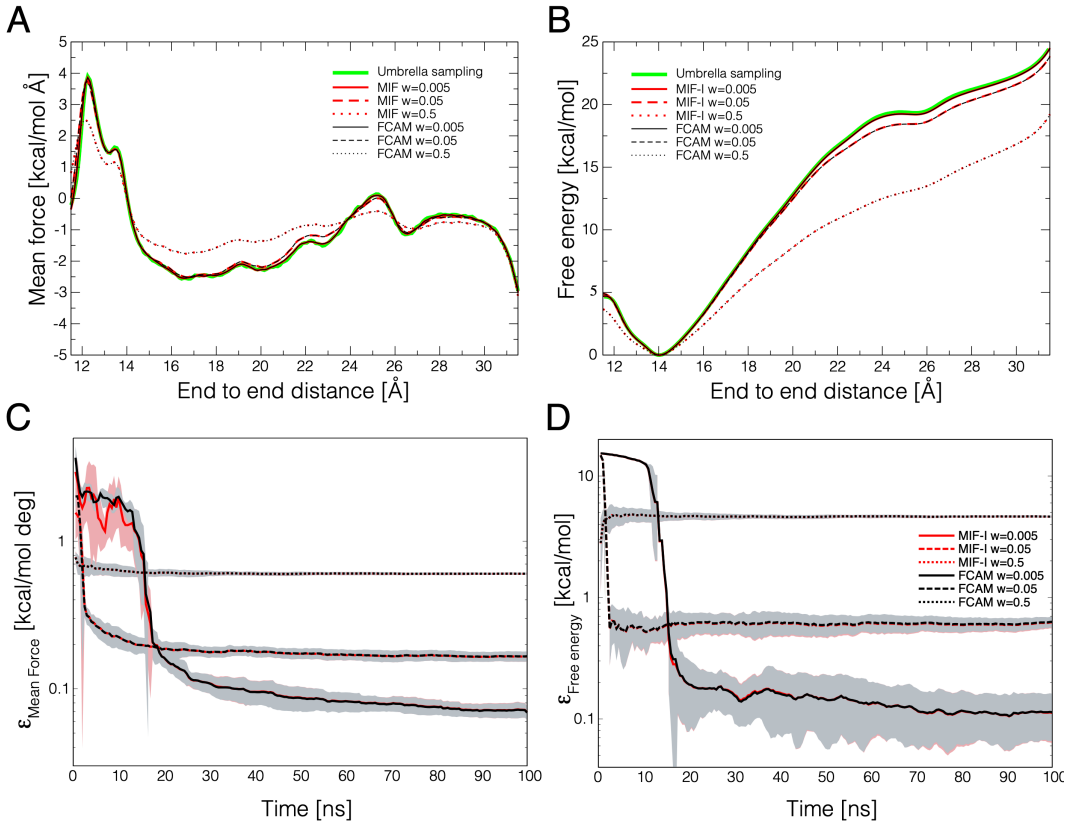

Figure 5 Effect of the bias potential time-fluctuations on accuracy and convergence rate of mean forces and free energies calculated from a one-dimensional metadynamics simulations on deca-L-alanine. All panels and quantities are organized and outlined as in Fig. 3 (see associated caption). Every profile in panel A and B is calculated from the combined sampling of 10 independent metadynamics trajectories of 100 ns each.

Two-dimensional free energy surfaces from concurrent one-dimensional biases

To assess the performance of the proposed methodology in the context of multiple one-dimensional biases applied to the same trajectory, we generated 10 independent simulations (of 30 ns each) on solvated butyramide using concurrent metadynamics (C-META) biases[29] to enhance sampling of both Φ and Ψ (Fig. 1). That is, two biasing potentials $V_1(\Phi, t)$ and $V_2(\Psi, t)$ are applied independently, and so the overall bias potential is $V(\Phi, \Psi, t) = V_1(\Phi, t) + V_2(\Psi, t)$. This type of biasing scheme produces a uniform distribution on Φ and Ψ individually, but owing to the correlations between these two CVs the corresponding two-dimensional space is not explored uniformly (Fig. S3). This implies that the overall bias potential, $V(\Phi, \Psi, t)$, does not compensate

the free energy surface along Φ and Ψ, and hence, it is not a free energy estimator. Similarly, the biasing potentials $V_1(\Phi, t)$ and $V_2(\Psi, t)$ do not compensate the individual projections of this free energy surface along either Φ or Ψ respectively. To verify whether the correct two-dimensional free energy can be nevertheless recovered with FCAM, we divided the space of Φ and Ψ in a regular grid of spacing 2.5° in each direction and for each grid point we calculated the mean force using Eq. 9; as in the previous section, we also calculated the mean instantaneous force (using Eq. 10) for comparison[60]. The density estimator was in both cases the product of two Gaussians of standard deviation 2.5°. Free energies were obtained from mean forces integration using KMC. The accuracy of the resulting mean forces and free energy was again assessed against the corresponding estimates derived from an US simulation of 130 ns. This US simulation used a static bias potential on Φ and Ψ deduced from a metadynamics simulation (of 75 ns) that applies an actual two-dimensional bias and that does explore uniformly the Φ, Ψ space. The two-dimensional free energy from US was estimated using standard histogram reweighting[13] from the US bias potential as detailed in the previous section (and using 2.5° bin spacing in Φ and Ψ). Owing to the low precision of finite differences, reference mean forces from US simulations were obtained from the local average of instantaneous forces (Eq. 10).

In Fig. 6AB we report mean-force surfaces for each Φ and Ψ component and the associated free energy landscape, obtained using Eq. 9 from the combined sampling of the C-META simulations. The mean-force surfaces are smooth and well-defined throughout, except near the central region ($(\Phi, \Psi) \sim (0,0)$ in Fig. 6A) which is poorly sampled (Fig. S3). Owing to the integration process, the effect of noisy forces is somewhat smoothed in the associated free energy landscape. Mean forces and free energies calculated from the C-META simulations generally feature excellent correlation with those obtained from US (Fig. 6CD), regardless of the type of estimate used (either from Eq. 9 or Eq. 10). Finally, the time dependence of forces and free energy errors (respect to US values), outlines that estimates derived with the proposed approach (FCAM in Fig. 6EF) converge with similar rate of the corresponding values calculated with instantaneous forces, according to Eq. 10 (MIF and MIF-I in Fig. 6EF).

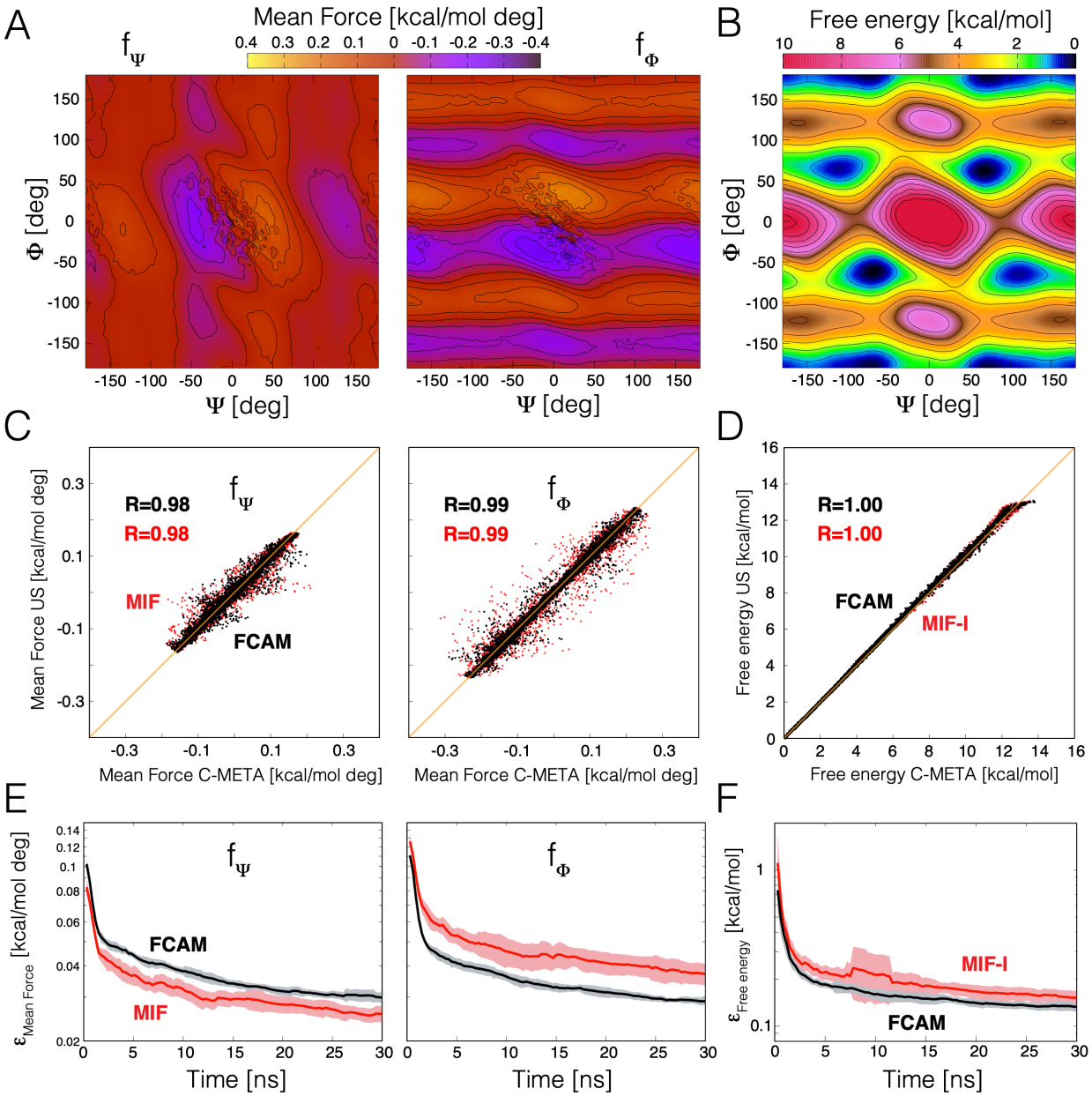

Figure 6. Assessment of convergence and accuracy of mean forces and free energy surfaces calculated with the proposed approach and mean instantaneous forces, from concurrent metadynamics (C-META) on the Φ and Ψ dihedral angles of butyramide. (A, B) Surfaces of mean forces components along Φ and Ψ (f_Φ, f_Ψ) and free energy as function of those dihedrals, obtained from 10 metadynamics simulations of 30 ns each, using Eq. 9 and KMC. Contour lines are drawn every 0.05 kcal/(mol deg) and 1 kcal/mol for mean foces and free energy surfaces respectively. (C,D) Correlation plot of mean forces and free energies calculated using Eq. 9 (FCAM) and Eq. 10 (MIF and MIF-I)[60] in reference to US estimates. (E, F) Time dependence of the error on mean forces and free energies for estimates based on Eq. 9 and Eq. 10. The error was calculated with respect to US estimates as explained in the caption of Fig. 1. Lines and shaded regions reflect average error and standard deviations over 10 independent metadynamics trajectories respectively.

Two-dimensional free-energy surfaces from coupled one-dimensional biases

A main goal of this work is to provide a robust methodology for computing multidimensional free energy landscapes from multiple simulations with adaptive biasing potentials applied to different CVs. For example, in bias-exchange (BE) metadynamics simulations[28], many metadynamics trajectories calculated in parallel, each applying biasing potentials on different CVs, are coupled to each other through a replica-exchange scheme. Multidimensional free energies from this type of simulations have been typically derived using WHAM (Eq. 4 and 5)[33], which is used in this case for comparative analysis. Here, we test the capability of the proposed approach to analyze BE simulations for the solvated alanine dipeptide. For this system, we performed BE simulations using two replicas; one biased on the Φ Ramachandran torsional angle and the other on Ψ (Fig. 7). To provide a performance assessment against different biasing schemes, we carried out two independent sets of BE simulations of 400 ns each (200 ns for each replica), using either standard (META) or well-tempered metadynamics (W-META; featuring a gradual reduction of the height of the added Gaussians)[18, 19, 48]. The results are compared with the free energy obtained from ~2 μs MD simulation, which was calculated according to Eq. 1 from the histogram along Φ and Ψ (bin spacing of 2.5^{o} in each direction). The two-dimensional free energy landscapes derived from MD and BE plus mean forces integration (from Eq. 9 and KMC) are reported in Fig. 7A, highlighting the marked resemblance between the two maps. This figure also illustrates how, owing the presence of the biasing potentials, BE is significantly more efficient than MD in sampling high free energy regions and thus crossing free energy barriers. Nonetheless, due to the application of mono dimensional biasing potentials, BE does not achieve uniform sampling of the Φ, Ψ space. In this case, we also show an example of minimum free-energy path between α_R and α_L conformations (Fig. 7A) obtained by maximizing the path probability in Eq. 14. Fig. 7B outlines how, regardless of the particular metadynamics variant used to perform the simulation, there is an excellent correlation between free energies calculated with MD and BE using mean forces integration, especially at low free energies where MD is accurate. WHAM also achieves overall a very good correlation with MD (right panel of Fig. 7B), nonetheless particularly for low free energy regions features larger discrepancies (regardless of the binning used) than mean forces integration (inset of Fig. 7B). The latter deviations are also apparent from the correlation plot.

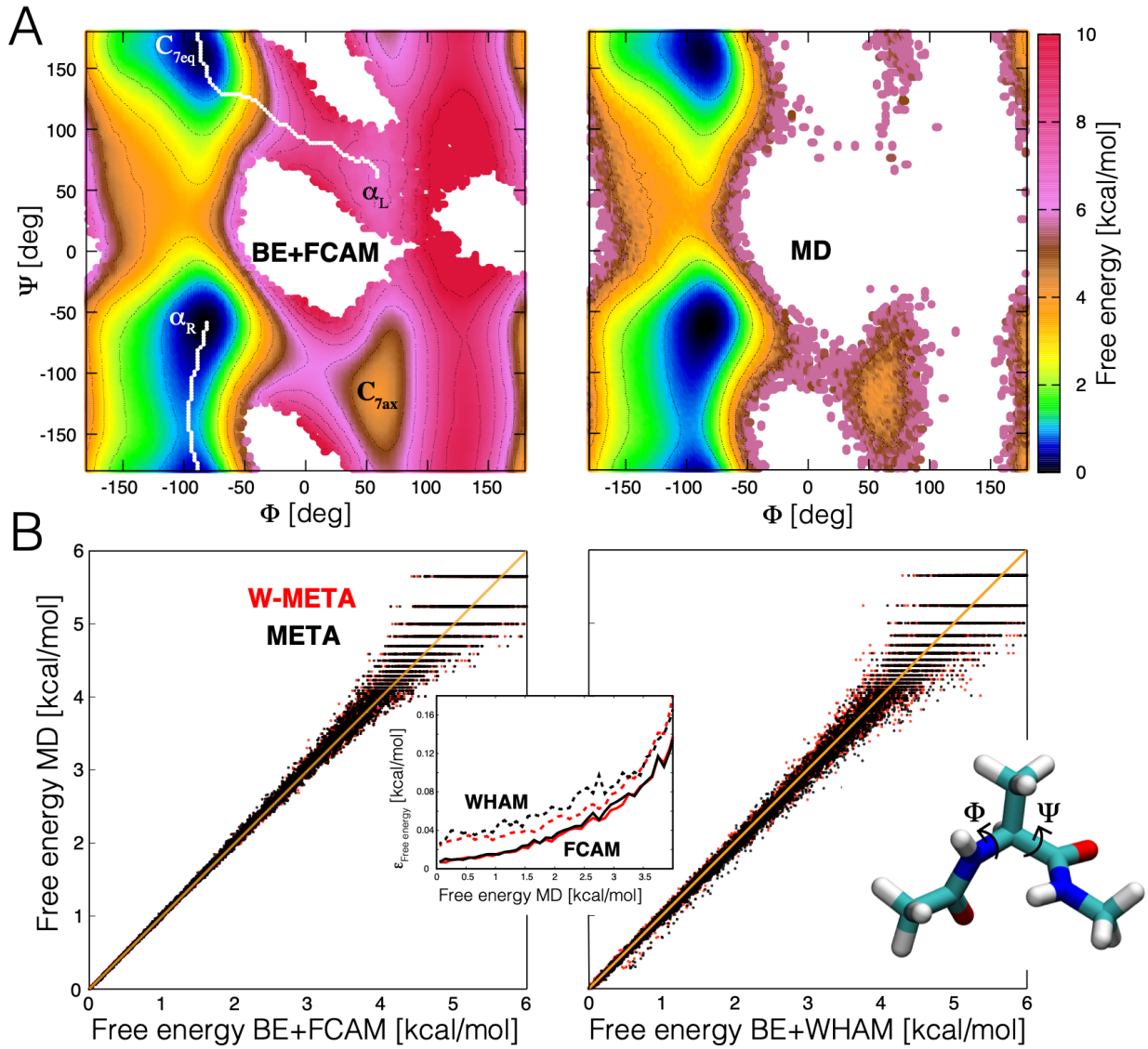

Figure 7. Comparative analysis of two-dimensional free energy landscapes of alanine dipeptide derived from MD and BE using either mean forces integration or WHAM. (A) Free energy map as a function of the Φ and Ψ dihedral angles of alanine dipeptide calculated using BE plus mean forces integration (left panel; BE simulations are performed using standard metadynamics) and MD (right panel). Contour lines are drawn with 1 kcal/mol spacings. The minimum free energy path connecting α_R and α_L conformations is shown as a white dotted line. (B) Correlation plot between MD and BE free energies, in which the latter are derived either from mean forces integration (left panel; Eq. 9 and KMC) or from WHAM (right panel). Data referred to BE simulation carried out using either conventional metadynamics (META) or the well-tempered variant (W-META) are shown as black and red circles respectively. The inset of panel B reports the absolute value of the difference between free energies calculated with MD and BE, using either mean forces (solid line) or WHAM (dashed line), as a function of the free energy from MD. Reported values correspond to a running average over intervals of 0.1 kcal/mol. Black and red lines refer to META and W-META simulations respectively.

High-dimensional free energy landscapes for both model and complex systems

In the previous sections we demonstrated that the proposed methodology provides an accurate framework to derive free energy landscapes in one and two dimensions across different biasing

schemes and model systems. However, for complex systems such as proteins it is rare that only one or two CVs define a mechanism or process, i.e. explain the so-called committor probabilities between relevant free energy minima[4, 6, 74]. Unless the CVs have been specifically optimized, e.g. so that they correctly capture all the slow degrees of freedom[23], a low dimensional description might merge together distinct conformations separated by barriers and/or underestimate the free energy of the latter[18]. Provided there is sufficient statistical sampling[75], a practical strategy to alleviate these problems is to increase the number of CVs used to calculate the free energy landscape. Additionally, even using optimal CVs[20-24], a high dimensional analysis is in same case strictly required to properly characterize the system under study, as for example to describe complex protein conformational transitions[30, 31].

To assess whether FCAM may be used to derive accurate free energy landscapes in multiple dimensions, we applied this methodology to study the isomerization of an Ace-Ala_3-Nme peptide[33]. For this system we performed ~1.5 μs BE metaydnamics simulations using six replicas (260 ns x 6), each biased with one of the six backbone dihedral angles shown in Fig. 8A. We then used the proposed approach (Eq. 9 and KMC) to analyze these simulations by calculating the six-dimensional free energy landscape as a function of all backbone dihedral angles. For comparison, the same landscape was also evaluated from ~6 μs MD simulation. To do so, we derived the six-dimensional probability density (see Eq. 1) based on the same Gaussian density estimator used for computing mean forces. Despite the high dimensionality and the fine description adopted (Gaussian standard deviation and bins side of 12°), there is an excellent correlation between the two free energies (R=0.97), especially at low free energy values where MD is accurate (Fig. 8A). The average discrepancy between the two types of estimate is 0.35 kcal/mol (see inset of Fig. 8A).

After corroborating the good performance of FCAM for high-dimensional analysis on a model system, we illustrate its application to a realistic case. In particular, we re-analyzed previously published BE simulations on the SH3-SH2 tandem of Abl kinase[50] (Fig. 8B). The latter tandem has been shown to primarily adopt the inhibitory or "on" conformation when engaged with catalytic domain and other elements, whereas X-ray crystallography[76] and MD simulations[50] revealed that it can adopt an alternative non-inhibitory, "off", conformation when isolated. These simulations comprise 32 simulations replicas (of 200 ns each) biased with different pair combinations of five total CVs. Two of these CVs monitor the relative position of protein (S1) or interdomain connector (S2) along a line connecting on and off conformations, while a third CV (S3) measures the distance from this line (in the case of S1). The other two CVs are pseudo dihedrals describing interdomain orientations. For this system we derived the free energy landscape as a function of all five CVs using mean forces integration (Eq. 9 and KMC). To visualize this landscape, we constructed its projection along S1, S2 and S3 (by integrating the probability density along the remaining CVs; Fig. 8B). Consistently with our previous analysis [50], this landscape is consistent with the notion that the isolated tandem adopts primarily the off conformation. The derived minimum free energy pathway between on and off conformations (Fig. 8BC) confirms the presence of a barrier of ~4 kcal/mol (Fig. 8C), in agreement with the

observation of spontaneous transitions between these two conformations during conventional MD simulations[50].

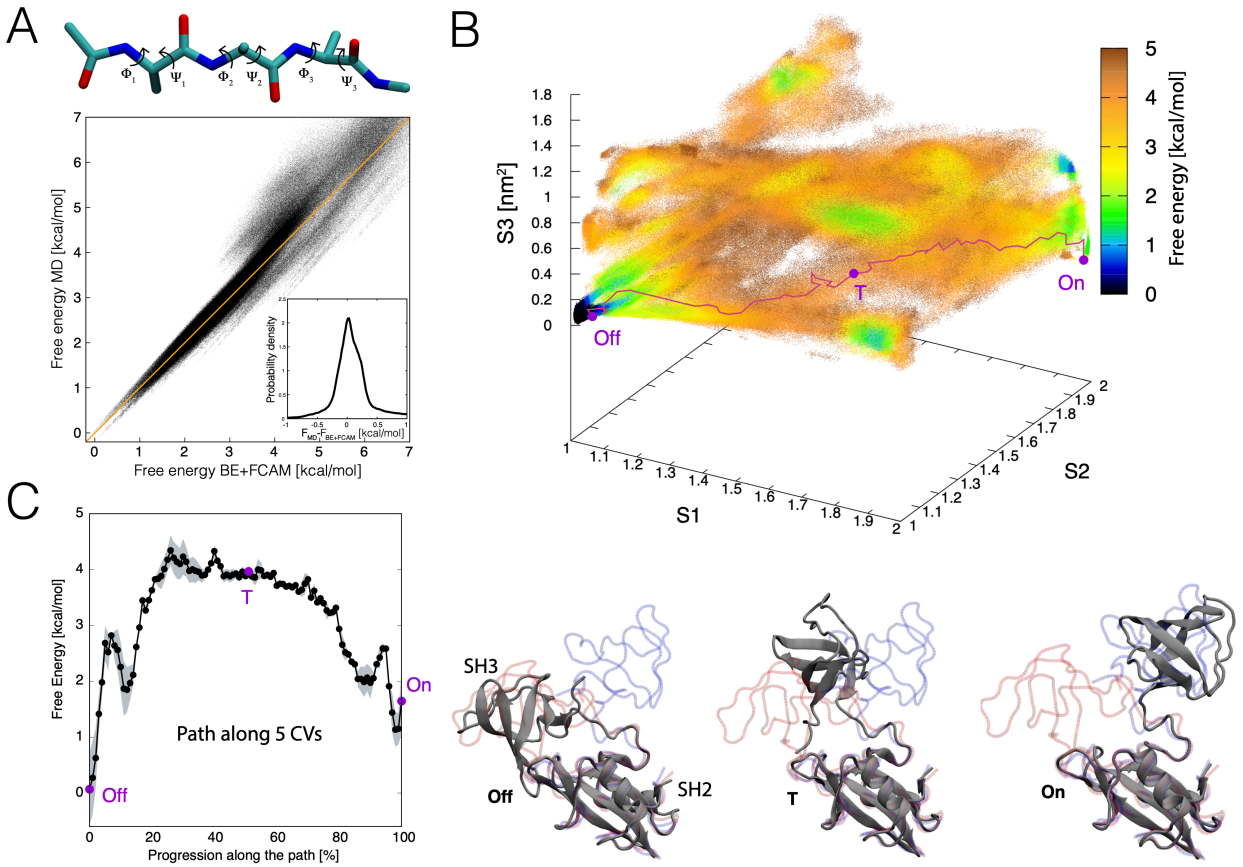

Figure 8. Application of FCAM to high dimensional cases. (A) Illustration of the Ace-Ala$_3$-Nme peptide and backbone dihedral angles (on panel top). Correlation plot of six-dimensional free energies obtained with standard MD and BE plus mean forces integration. Mean forces were calculated (using Eq. 9) on a regular grid of 12° spacing in each direction, leading to ~2.5 millions grid points. The free energy from MD was obtained constructing the six-dimensional probability density on the same bin points using a Gaussian density estimator (same used in Eq. 9). The inset reports the histogram of the deviations between free energy estimates from MD and BE plus mean forces integration. (B) Free energy landscape of SH2-SH3 tandem of Abl kinase, as a function of S1, S2 and S3 CVs (see main text). The landscape was obtained projecting the five-dimensional free energy on S1, S2 and S3. The minimum free energy pathway (see Eq. 14) connecting on and off states is shown by a red line, while indicated reference configurations (purple circles) are shown on the bottom of the panel in cartoon representation. The reference X-ray structures of on and off states are outlined by the blue and red tubular representations respectively. (C) Minimum free energy pathway connecting on and off states of Abl kinase. The shaded area reflects the standard error obtained through blocks averages.

Conclusions

In this work we have introduced a methodology for the calculation of multidimensional free energy landscapes for complex molecular systems, which we refer to as Force Correction Analysis Method (FCAM). This approach builds on concepts outlined in previous studies, such as umbrella integration[41] and its variants[42-45], and entails a post-hoc derivation of unbiased estimates of free energy gradients or mean forces from simulation samples obtained with multiple adaptively-

biased MD simulations. Through a series of applications to both simple and complex systems we demonstrated that, unlike existing approaches, this methodology provides a unified, self-consistent framework to derive thermodynamic quantities from these kinds of enhanced-sampling simulations. FCAM may be used with protocols based on either single or multiple trajectories, carried out independently or coupled through an exchange scheme, and implementing biases on the same or different collective variables (CVs). The methodology relies on local averages to calculate the mean forces; hence, its practical application is straightforward and requires only quantities that can be calculated readily or that are already made available by simulation programs. Correct application of this analysis method however requires that the simulation data be obtained with biases that do not change abruptly or too frequently so that the molecular system remains close to equilibrium. Here we illustrated the application of the proposed approach to up six-dimensions. Practical analysis with higher dimensions can be carried out provided that there is enough sampling to perform accurate local averages in connected regions of the CVs space. A significant improvement in this regard can be provided by using specifically tuned estimators of the probability density[30].

For the systems analyzed in this work, the proposed approach showed similar accuracy and convergence rate of an alternative energetic analysis that relies on the calculation of instantaneous forces[14-16, 58-60], which, however, are not available for every type of CV and simulation setup. Furthermore, consistently with previous applications of mean forces-based approaches[41], we observed reduced statistical error compared to the weighted histogram analysis method (WHAM)[32, 33, 41]. A disadvantage compared to WHAM[33], however, is that the free energy can be directly derived only a as function of a set of CVs which encompasses the ones on which the biasing potentials are applied. This notwithstanding, owing to the effect of the bias potential, the sampling along those CVs is significantly improved compared to any other direction, hence, evaluated mean forces and free energies are expected to be more accurate along the latter variables. We showed that the free energy as a function of any other set of CVs or unbiased ensemble averages can be inferred from post hoc ensemble reweighting based on the free energy calculated along the initial set of CVs.

In conclusion, we anticipate that FCAM will greatly facilitate quantitative mechanistic analysis of complex processes in chemical and biological systems. The overall methodology, including the kinetic Monte Carlo scheme used to obtain free energies from the mean forces and to calculate minimum-energy paths, are implemented in python programs that will become freely available through GitHub.

Acknowledgements

This work was funded by the Division of Intramural Research of the National Heart, Lung and Blood Institute (NHLBI), National Institutes of Health (USA). Computational resources were in part provided by the NIH high-performance computing facility Biowulf.

References

1. Hollingsworth, S.A. and R.O. Dror, *Molecular Dynamics Simulation for All.* Neuron, 2018. **99**(6): p. 1129-1143.
2. Best, R.B. and K. Lindorff-Larsen, *Editorial overview: Theory and simulation: Interpreting experimental data at the molecular level.* Curr Opin Struct Biol, 2018. **49**: p. iv-v.
3. Gapsys, V. and B.L. de Groot, *On the importance of statistics in molecular simulations for thermodynamics, kinetics and simulation box size.* Elife, 2020. **9**.
4. Ma, A. and A.R. Dinner, *Automatic method for identifying reaction coordinates in complex systems.* Journal of Physical Chemistry B, 2005. **109**(14): p. 6769-6779.
5. Berezhkovskii, A. and A. Szabo, *One-dimensional reaction coordinates for diffusive activated rate processes in many dimensions.* Journal of Chemical Physics, 2005. **122**(1).
6. Best, R.B. and G. Hummer, *Reaction coordinates and rates from transition paths.* Proceedings of the National Academy of Sciences of the United States of America, 2005. **102**(19): p. 6732-6737.
7. Chipot, C. and A. Pohorille, *Free Energy Calculations*. Springer Series in Chemical Physics. 2007: Springer-Verlag Berlin Heidelberg.
8. Wolynes, P.G., J.N. Onuchic, and D. Thirumalai, *Navigating the Folding Routes.* Science, 1995. **267**(5204): p. 1619-1620.
9. Dill, K.A. and H.S. Chan, *From Levinthal to pathways to funnels.* Nature Structural Biology, 1997. **4**(1): p. 10-19.
10. Onuchic, J.N., et al., *The energy landscape theory of protein folding: Insights into folding mechanisms and scenarios.* Advances in Protein Chemistry, Vol 53, 2000. **53**: p. 87-152.
11. Gfeller, D., et al., *Complex network analysis of free-energy landscapes.* Proc Natl Acad Sci U S A, 2007. **104**(6): p. 1817-22.
12. Peters, B., *Reaction rate theory and rare events*. 2017, Amsterdam, Netherlands: Elsevier. 634.
13. Torrie, G.M. and J.P. Valleau, *Non-Physical Sampling Distributions in Monte-Carlo Free-Energy Estimation - Umbrella Sampling.* Journal of Computational Physics, 1977. **23**(2): p. 187-199.
14. Darve, E. and A. Pohorille, *Calculating free energies using average force.* Journal of Chemical Physics, 2001. **115**(20): p. 9169-9183.
15. Henin, J. and C. Chipot, *Overcoming free energy barriers using unconstrained molecular dynamics simulations.* Journal of Chemical Physics, 2004. **121**(7): p. 2904-2914.
16. Comer, J., et al., *The adaptive biasing force method: everything you always wanted to know but were afraid to ask.* J Phys Chem B, 2015. **119**(3): p. 1129-51.
17. Laio, A. and M. Parrinello, *Escaping free-energy minima.* Proc Natl Acad Sci U S A, 2002. **99**(20): p. 12562-6.
18. Laio, A. and F.L. Gervasio, *Metadynamics: a method to simulate rare events and reconstruct the free energy in biophysics, chemistry and material science.* Reports on Progress in Physics, 2008. **71**(12).
19. Bussi, G. and A. Laio, *Using metadynamics to explore complex free-energy landscapes.* Nature Reviews Physics, 2020. **2**(4): p. 200-212.
20. Peters, B. and B.L. Trout, *Obtaining reaction coordinates by likelihood maximization.* Journal of Chemical Physics, 2006. **125**(5).

21. Branduardi, D., F.L. Gervasio, and M. Parrinello, *From A to B in free energy space.* J Chem Phys, 2007. **126**(5): p. 054103.
22. Diaz Leines, G. and B. Ensing, *Path finding on high-dimensional free energy landscapes.* Phys Rev Lett, 2012. **109**(2): p. 020601.
23. Tiwary, P. and B.J. Berne, *Spectral gap optimization of order parameters for sampling complex molecular systems.* Proceedings of the National Academy of Sciences of the United States of America, 2016. **113**(11): p. 2839-2844.
24. Ribeiro, J.M.L., et al., *Reweighted autoencoded variational Bayes for enhanced sampling (RAVE).* Journal of Chemical Physics, 2018. **149**(7).
25. Maragliano, L. and E. Vanden-Eijnden, *A temperature accelerated method for sampling free energy and determining reaction pathways in rare events simulations.* Chemical Physics Letters, 2006. **426**(1-3): p. 168-175.
26. Marinelli, F., *Following Easy Slope Paths on a Free Energy Landscape: The Case Study of the Trp-Cage Folding Mechanism.* Biophysical Journal, 2013. **105**(5): p. 1236-1247.
27. Pfaendtner, J. and M. Bonomi, *Efficient Sampling of High-Dimensional Free-Energy Landscapes with Parallel Bias Metadynamics.* Journal of Chemical Theory and Computation, 2015. **11**(11): p. 5062-5067.
28. Piana, S. and A. Laio, *A bias-exchange approach to protein folding.* J Phys Chem B, 2007. **111**(17): p. 4553-9.
29. Gil-Ley, A. and G. Bussi, *Enhanced Conformational Sampling Using Replica Exchange with Collective-Variable Tempering (vol 11, pg 1077, 2015).* Journal of Chemical Theory and Computation, 2015. **11**(11): p. 5554-5554.
30. Rodriguez, A., et al., *Computing the Free Energy without Collective Variables.* J Chem Theory Comput, 2018. **14**(3): p. 1206-1215.
31. Sormani, G., A. Rodriguez, and A. Laio, *Explicit Characterization of the Free-Energy Landscape of a Protein in the Space of All Its Calpha Carbons.* J Chem Theory Comput, 2020. **16**(1): p. 80-87.
32. Kumar, S., et al., *Multidimensional Free-Energy Calculations Using the Weighted Histogram Analysis Method.* Journal of Computational Chemistry, 1995. **16**(11): p. 1339-1350.
33. Marinelli, F., et al., *A kinetic model of trp-cage folding from multiple biased molecular dynamics simulations.* PLoS Comput Biol, 2009. **5**(8): p. e1000452.
34. Biarnes, X., et al., *METAGUI. A VMD interface for analyzing metadynamics and molecular dynamics simulations.* Computer Physics Communications, 2012. **183**(1): p. 203-211.
35. Crespo, Y., et al., *Metadynamics convergence law in a multidimensional system.* Physical Review E, 2010. **81**(5).
36. Branduardi, D., G. Bussi, and M. Parrinello, *Metadynamics with Adaptive Gaussians.* Journal of Chemical Theory and Computation, 2012. **8**(7): p. 2247-2254.
37. Rosta, E. and G. Hummer, *Free Energies from Dynamic Weighted Histogram Analysis Using Unbiased Markov State Model.* Journal of Chemical Theory and Computation, 2015. **11**(1): p. 276-285.
38. Stelzl, L.S., et al., *Dynamic Histogram Analysis To Determine Free Energies and Rates from Biased Simulations.* J Chem Theory Comput, 2017. **13**(12): p. 6328-6342.
39. Wu, H., et al., *Statistically optimal analysis of state-discretized trajectory data from multiple thermodynamic states.* Journal of Chemical Physics, 2014. **141**(21).

40. Wu, H., et al., *Multiensemble Markov models of molecular thermodynamics and kinetics.* Proceedings of the National Academy of Sciences of the United States of America, 2016. **113**(23): p. E3221-E3230.
41. Kastner, J. and W. Thiel, *Bridging the gap between thermodynamic integration and umbrella sampling provides a novel analysis method: "Umbrella integration".* J Chem Phys, 2005. **123**(14): p. 144104.
42. Zheng, L.Q. and W. Yang, *Practically Efficient and Robust Free Energy Calculations: Double-Integration Orthogonal Space Tempering.* Journal of Chemical Theory and Computation, 2012. **8**(3): p. 810-823.
43. Fu, H.H., et al., *Extended Adaptive Biasing Force Algorithm. An On-the-Fly Implementation for Accurate Free-Energy Calculations.* Journal of Chemical Theory and Computation, 2016. **12**(8): p. 3506-3513.
44. Lesage, A., et al., *Smoothed Biasing Forces Yield Unbiased Free Energies with the Extended-System Adaptive Biasing Force Method.* Journal of Physical Chemistry B, 2017. **121**(15): p. 3676-3685.
45. Marinova, V. and M. Salvalaglio, *Time-independent free energies from metadynamics via mean force integration.* J Chem Phys, 2019. **151**(16): p. 164115.
46. Vaneerden, J., et al., *Potential of Mean Force by Thermodynamic Integration - Molecular-Dynamics Simulation of Decomplexation.* Chemical Physics Letters, 1989. **164**(4): p. 370-376.
47. Maragliano, L. and E. Vanden-Eijnden, *Single-sweep methods for free energy calculations.* Journal of Chemical Physics, 2008. **128**(18).
48. Barducci, A., G. Bussi, and M. Parrinello, *Well-tempered metadynamics: A smoothly converging and tunable free-energy method.* Physical Review Letters, 2008. **100**(2).
49. Marinelli, F., et al., *Evidence for an allosteric mechanism of substrate release from membrane-transporter accessory binding proteins.* Proc Natl Acad Sci U S A, 2011. **108**(49): p. E1285-92.
50. Corbi-Verge, C., et al., *Two-state dynamics of the SH3-SH2 tandem of Abl kinase and the allosteric role of the N-cap.* Proceedings of the National Academy of Sciences of the United States of America, 2013. **110**(36): p. E3372-E3380.
51. Liao, J., et al., *Mechanism of extracellular ion exchange and binding-site occlusion in a sodium/calcium exchanger.* Nat Struct Mol Biol, 2016. **23**(6): p. 590-599.
52. Ono, J. and H. Nakai, *Weighted histogram analysis method for multiple short-time metadynamics simulations.* Chemical Physics Letters, 2020. **751**.
53. Bonomi, M., et al., *PLUMED: A portable plugin for free-energy calculations with molecular dynamics.* Computer Physics Communications, 2009. **180**(10): p. 1961-1972.
54. Tribello, G.A., et al., *PLUMED 2: New feathers for an old bird.* Computer Physics Communications, 2014. **185**(2): p. 604-613.
55. Bonomi, M., et al., *Promoting transparency and reproducibility in enhanced molecular simulations.* Nature Methods, 2019. **16**(8): p. 670-673.
56. Fiorin, G., M.L. Klein, and J. Henin, *Using collective variables to drive molecular dynamics simulations.* Molecular Physics, 2013. **111**(22-23): p. 3345-3362.
57. Sidky, H., et al., *SSAGES: Software Suite for Advanced General Ensemble Simulations.* Journal of Chemical Physics, 2018. **148**(4).
58. Carter, E.A., et al., *Constrained Reaction Coordinate Dynamics for the Simulation of Rare Events.* Chemical Physics Letters, 1989. **156**(5): p. 472-477.

59. Ciccotti, G., R. Kapral, and E. Vanden-Eijnden, *Blue moon sampling, vectorial reaction coordinates, and unbiased constrained dynamics.* Chemphyschem, 2005. **6**(9): p. 1809-1814.
60. Henin, J., et al., *Exploring Multidimensional Free Energy Landscapes Using Time-Dependent Biases on Collective Variables.* Journal of Chemical Theory and Computation, 2010. **6**(1): p. 35-47.
61. Phillips, J.C., et al., *Scalable molecular dynamics with NAMD.* Journal of Computational Chemistry, 2005. **26**(16): p. 1781-1802.
62. Phillips, J.C., et al., *Scalable molecular dynamics on CPU and GPU architectures with NAMD.* Journal of Chemical Physics, 2020. **153**(4).
63. Maragliano, L., et al., *String method in collective variables: minimum free energy paths and isocommittor surfaces.* J Chem Phys, 2006. **125**(2): p. 24106.
64. Harland, B. and S.X. Sun, *Path ensembles and path sampling in nonequilibrium stochastic systems.* J Chem Phys, 2007. **127**(10): p. 104103.
65. MacKerell, A.D., et al., *All-atom empirical potential for molecular modeling and dynamics studies of proteins.* Journal of Physical Chemistry B, 1998. **102**(18): p. 3586-3616.
66. Mackerell, A.D., M. Feig, and C.L. Brooks, *Extending the treatment of backbone energetics in protein force fields: Limitations of gas-phase quantum mechanics in reproducing protein conformational distributions in molecular dynamics simulations.* Journal of Computational Chemistry, 2004. **25**(11): p. 1400-1415.
67. Hustedt, E.J., et al., *Confidence Analysis of DEER Data and Its Structural Interpretation with Ensemble-Biased Metadynamics.* Biophys J, 2018. **115**(7): p. 1200-1216.
68. Hess, B., et al., *GROMACS 4: Algorithms for Highly Efficient, Load-Balanced, and Scalable Molecular Simulation.* J Chem Theory Comput, 2008. **4**(3): p. 435-47.
69. Duan, Y., et al., *A point-charge force field for molecular mechanics simulations of proteins based on condensed-phase quantum mechanical calculations.* Journal of Computational Chemistry, 2003. **24**(16): p. 1999-2012.
70. Laio, A., et al., *Assessing the accuracy of metadynamics.* Journal of Physical Chemistry B, 2005. **109**(14): p. 6714-6721.
71. Bussi, G., A. Laio, and M. Parrinello, *Equilibrium free energies from nonequilibrium metadynamics.* Physical Review Letters, 2006. **96**(9).
72. Park, S., et al., *Free energy calculation from steered molecular dynamics simulations using Jarzynski's equality.* Journal of Chemical Physics, 2003. **119**(6): p. 3559-3566.
73. Raiteri, P., et al., *Efficient reconstruction of complex free energy landscapes by multiple walkers metadynamics.* Journal of Physical Chemistry B, 2006. **110**(8): p. 3533-3539.
74. Ren, W., et al., *Transition pathways in complex systems: Application of the finite-temperature string method to the alanine dipeptide.* Journal of Chemical Physics, 2005. **123**(13).
75. Scott, D.W., *Multivariate density estimation: theory, practice, and visualization*. 2015., John Hoboken, NJ, USA: Wiley & Sons.
76. Fushman, D., R. Xu, and D. Cowburn, *Direct determination of changes of interdomain orientation on ligation: Use of the orientational dependence of N-15 NMR relaxation in Abl SH(32).* Biochemistry, 1999. **38**(32): p. 10225-10230.